Eddy Amplitudes and Fluxes in a Homogeneous Model of Fully Developed Baroclinic Instability

VITALY D. LARICHEV

Program in Atmospheric and Oceanic Sciences, Princeton University, Princeton, New Jersey

ISAAC M. HELD

Geophysical Fluid Dynamics Laboratory/NOAA, Princeton, New Jersey

(Manuscript received 25 July 1994, in final form 7 March 1995)

ABSTRACT

A horizontally homogeneous two-layer quasigeostrophic model with imposed environmental vertical shear is used to study eddy energies and fluxes in the regime in which an inverse barotropic energy cascade excites eddies of much larger scale than the deformation radius. It is shown that the eddy potential vorticity flux, "thickness" flux, and the extraction of energy from the background flow are dominated by the largest eddies excited by the cascade, and not by deformation-scale eddies. The role of the latter is a catalytic one of transferring the baroclinic energy cascading downscale into the barotropic mode, thereby energizing the inverse cascade.

Based on this picture, scaling arguments are developed for the eddy energy level and potential vorticity flux in statistical equilibrium. The potential vorticity flux can be thought of as generated by a diffusivity of magnitude Uk_d/k_0^2, where U is the difference between the mean currents in the two layers, k_d is the inverse of the deformation radius, and k_0 is the wavenumber of the energy-containing eddies. This result is closely related to that proposed by Green, although the underlying dynamical picture is different.

1. Introduction

In a baroclinically unstable system one anticipates eddy activity on the scale of the internal Rossby deformation radius. In a large enough system, one can hope for a separation between this "mesoscale" and larger scales of interest that would facilitate the development of parameterization schemes for the mesoscale eddy fluxes, particularly for the eddy potential vorticity flux, which is the central quantity of interest when considering the effects of these eddies on larger scales. However, one also has to reckon with the existence of an inverse energy cascade that has the potential for filling in this gap in length scales. In this paper we are concerned with understanding how the eddy amplitudes and fluxes are determined in a system in which mechanisms that might halt this cascade, such as the beta-effect, scattering by topography, or boundary layer friction, are sufficiently weak that the inverse cascade proceeds through a substantial range of scales.

Of principal concern is the question of which scales dominate the potential vorticity flux in this kind of strongly nonlinear, baroclinically unstable system. Equivalently, one can ask which scales dominate the extraction of energy from the environmental available potential energy reservoir. Linear theory tells us that deformation-scale waves are the most unstable disturbances, which leads one to suspect that they might also dominate the energy production. But countering this expectation is the simple fact that the spectral shape consistent with the barotropic inverse energy cascade results in a peak in energy at the scale at which this cascade halts, not at the scale at which energy is injected into the barotropic flow. What is to prevent these large energy-containing eddies from advecting potential vorticity downgradient and dominating the flux and the energy generation, which is proportional to the potential vorticity flux? This question is made more compelling by the argument of Rhines (1977) and Salmon (1978, 1980) that the flow will be predominately barotropic on large scales, so that the dynamics of the baroclinic part of the flow, on scales much larger than the radius of deformation, will reduce to the advection of the *baroclinic* potential vorticity by the *barotropic* flow. Since this potential vorticity does not directly induce the flow field that is responsible for the advection, it must act essentially as a passive tracer, so it is difficult to see how the flux could fail to be dominated by the energy-containing eddies.

There are several studies of the statistically steady states of baroclinically unstable flows that show that

Corresponding author address: Dr. Vitaly D. Larichev, Program in Atmospheric and Oceanic Sciences, NOAA/ERL/GFD, Princeton University, P.O. Box CN710, Sayre Hall, Princeton, NJ 08544-0710. E-mail: vdl@gfdl.gov.

the energy generation moves to larger scales when the energy moves to larger scales, but the difference in scales is never very large. In the context of homogeneous turbulence models of the sort examined here, this tendency can be seen in Held and O'Brien (1992) and Panetta (1993). Our intention here is to study a system in which the scale separation between the energy-containing eddies and the deformation radius is very clear, to determine if the energy-containing eddies dominate the flux and energy production or if the deformation-scale eddies continue to contribute significantly.

We address this problem by examining a numerical two-layer model in a doubly periodic domain with an imposed background vertical current (wind) shear. The results are interpreted in terms of the energy cascades expected in such a model from the work of Rhines (1977), Salmon (1978, 1980), and Hoyer and Sadourny (1982). The analysis leads to a scaling argument for the magnitude of the potential vorticity (or thickness) flux, or baroclinic energy production, in such a system. The numerical model is introduced in section 2, numerical results are described in section 3, and theoretical interpretation of these results is provided in section 4.

2. The model

We consider the flat-bottom, rigid-lid quasigeostrophic two-layer model on an f plane, governed by 2D advection of potential vorticity Q_i, subject to dissipation at small and large scales:

$$\partial Q_1/\partial t + J(\Psi_1, Q_1) = -\nu\nabla^8 Q_1 \quad (1a)$$

$$\partial Q_2/\partial t + J(\Psi_2, Q_2) = -\nu\nabla^8 Q_2 - \kappa\nabla^2\Psi_2. \quad (1b)$$

Subscripts 1 and 2 refer to the upper and lower layers, respectively; J is the horizontal Jacobian and ∇^2 the horizontal Laplacian operator. The potential vorticities Q_i and the velocities (u_i, v_i) are defined in terms of the streamfunctions Ψ_i:

$$Q_1 = \nabla^2\Psi_1 + k_d^2(\Psi_2 - \Psi_1)/2,$$

$$Q_2 = \nabla^2\Psi_2 + k_d^2(\Psi_1 - \Psi_2)/2,$$

$$(u_i, v_i) = (-\partial\Psi_i/\partial y, \partial\Psi_i/\partial x), \quad i = 1, 2, \quad (2)$$

where the depths of the layers are chosen equally and k_d^{-1} is the (internal) deformation radius. The large-scale dissipation, $-\kappa\nabla^2\Psi_2$, in (1) simulates friction in the Ekman layer at the bottom, while the ∇^8 term removes the enstrophy cascading to small scales.

We assume that the source of energy for the motion is the potential energy of a stationary, horizontally uniform flow with a vertical shear, that is, with uniform north–south interface slope:

$$\Psi_1 = -Uy + \psi_1(x, y, t),$$

$$\Psi_2 = Uy + \psi_2(x, y, t), \quad U = \text{const}; \quad (3)$$

ψ_1 and ψ_2 are required to be periodic over the square domain $0 \leq x, y \leq 2\pi$ so that $(k_x, k_y)_{\min} = 1$, implying a scaling of the spatial dimensions by $(2\pi)^{-1}$ times the domain size. Closely related models have been studied by Rhines (1977), Salmon (1978, 1980), Haidvogel and Held (1980), Vallis (1983), and Panetta (1993).

The model is solved with a standard spectral technique, transforming to a grid for the computation of quadratic products, using enough grid points to avoid aliasing. A leapfrog step with a weak Robert filter to eliminate any tendency for time splitting is used for the time integrations. We retain 256 Fourier harmonics in each spatial coordinate, so that $(k_x, k_y)_{\max} = 128$, and choose $k_d = 50$ with oceanic applications in mind. With this choice, we hope to resolve the dynamics near the radius of deformation, at least marginally, while leaving room for a substantial inverse cascade.

We set $U = 0.005$, so that the eddy energies are O(1) in the calculation described below. The Ekman damping coefficient is set equal to 0.04. This value leaves the flow sufficiently inviscid that the inverse energy cascade reaches the domain scale, while providing the damping on these largest scales needed to equilibrate the flow in a reasonable time. Using several trial integrations as a guide, we choose the diffusivity ν as small as possible while still preventing a buildup of enstrophy on small scales. The resulting value is 0.512×10^{-15}. Haidvogel and Held (1980) discuss the sensitivity of this model to the strength of the subgrid-scale damping, but in a different part of parameter space and at lower resolution.

Decomposing into barotropic and baroclinic vertical modes, $\psi = (\psi_1 + \psi_2)/2$, $\tau = (\psi_1 - \psi_2)/2$, the governing equations (1) become

$$\partial\nabla^2\psi/\partial t + J(\psi, \nabla^2\psi) + J(\tau, \nabla^2\tau) + U\partial\nabla^2\tau/\partial x = -\kappa\nabla^2(\psi - \tau)/2 - \nu\nabla^8(\nabla^2\psi) \quad (4a)$$

$$\partial(\nabla^2\tau - k_d^2\tau)/\partial t + J(\psi, \nabla^2\tau - k_d^2\tau) + J(\tau, \nabla^2\psi) + U\partial\nabla^2\psi/\partial x + Uk_d^2\partial\psi/\partial x = -\kappa\nabla^2(\tau - \psi)/2 - \nu\nabla^8(\nabla^2\tau - k_d^2\tau). \quad (4b)$$

3. Results

The model is initialized with very low amplitudes and random phases in all Fourier modes, so that the evolution starts with a linear stage of baroclinic instability. Amplitudes are chosen so that the isotropic barotropic and baroclinic energy spectra are independent of k: $E_\psi(k, 0) = E_\tau(k, 0) = 0.6 \times 10^{-7}$. Our notation is such that

$$\langle|\nabla\psi|^2\rangle = \int_0^\infty E_\psi(k, t)dk = \int_0^\infty k^2|\psi_k|^2 dk$$

$$\langle|\nabla\tau|^2 + k_d^2\tau^2\rangle = \int_0^\infty E_\tau(k, t)dk$$

$$= \int_0^\infty (k^2 + k_d^2)|\tau_k|^2 dk,$$

where $\langle \ldots \rangle$ is the area-averaged value so that the integrals over $E_\psi(k)$ and $E_\tau(k)$ are actually *twice* the barotropic and baroclinic energy.

The linear stage of baroclinic instability is observed until $t \approx 40$. (Linear theory predicts the maximal growth rate $\alpha_{\max}$ at $k_x = 0.64k_d \sim 32$, $k_y = 0$, with e-folding time $1/\alpha_{\max} = 4.8$.) During this period the nonlinear intermode exchange is small, and for $k \in [0, 40]$ there is nearly perfect correlation between τ and the barotropic meridional velocity v_ψ.

Starting at $t \approx 50$ the nonlinear terms become comparable to linear ones, at first for $k \in [20, 50]$. In (4a) the baroclinic term $J(\tau, \nabla^2\tau)$ becomes and remains dominant over the linear term $U\partial\nabla^2\tau/\partial x$ as the major forcing for the barotropic mode. Simultaneously, the correlation between τ and v_ψ starts to deteriorate in the same k range. The baroclinic energy production $Uk_d^2\overline{\tau v_\psi}$ (an overbar denotes an angular average in k space) becomes less efficient for those k, shifting the energy source to larger scales where this process repeats. The movement of the production proceeds (Fig. 1) until it reaches the largest scales, where equilibration is eventually achieved at $t \approx 500$. The shift of the production to large scales is accompanied by an increase in its total value. A key feature of the final equilibrated state is that the energy production at scales comparable to the deformation radius is negligible.

The flow at equilibrium exhibits long-period oscillations (Fig. 2a). The eddy turn-around time $T_e(k) = 2\pi k^{-1}(kE_\psi(k))^{-1/2}$ is determined by the barotropic velocities. From Fig. 4a, an estimate of this timescale for the gravest mode is $T_e(1) \approx 10$. The variability in the large scales is clearest in the baroclinic mode. The Ekman damping in the model is mechanical, but most of the energy in the baroclinic mode on large scales is potential rather than kinetic, so this mode is very weakly damped and must respond to the volatility of the production term (Fig. 2a). In contrast, the barotropic mode displays more regular behavior, not only due to the inertia resulting from its greater energy, but also due to the smaller variability in the intermode exchange, which serves as the energy source for this mode.

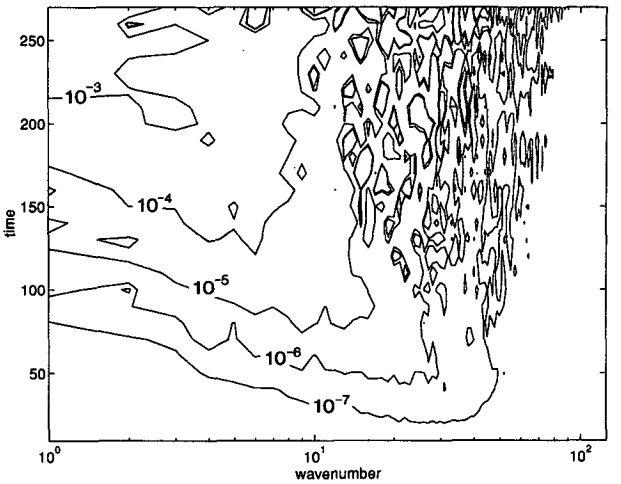

FIG. 1. The spectral structure of the energy production rate $Uk_d^2\overline{\tau v_\psi}$ as a function of time in the model spinup stage. The overbar refers to an angular average in wavenumber space.

Snapshots of the instantaneous baroclinic and barotropic potential vorticity in equilibrium are displayed in Fig. 3 (the baroclinic potential vorticity includes the contribution from the mean interface slope). The barotropic and baroclinic modes clearly have different dynamics. At scales larger than the deformation scale, the barotropic flow displays an hierarchy of circular vortices, which tend to get fewer and more isolated as the scale increases, making the picture look very similar to that which emerges with strictly 2D dynamics. At smaller scales, the enstrophy direct cascade becomes evident as it deforms the potential vorticity fields into thin, stretched filaments. This description is typical except during periods when injection of energy into the barotropic mode is less intense (see Fig. 2a), during which there are fewer deformation-scale vortices. The baroclinic mode clearly bears an imprint of those strong barotropic vortices as they distort and wrap up advectively the mean meridional temperature gradient. The baroclinic mode has the appearance of a tracer being advected passively at all scales with long, stretched filaments, which are an indication of a direct cascade [cf. Fig. 2 in Holloway and Kristmannsson (1984), which compares the potential vorticity and passive scalar fields in a simulated 2D flow].

The modal energy budget in wavenumber space follows from the dynamical equations (4):

$$\partial[(k^2 + l^2)|\psi_{k,l}|^2/2]/\partial t = \underbrace{\mathrm{Re}[\psi^*_{k,l}J_{k,l}(\psi, \nabla^2\psi)]}_{\mathrm{I}} + \underbrace{\mathrm{Re}[\psi^*_{k,l}J_{k,l}(\tau, \nabla^2\tau)]}_{\mathrm{II}} + \underbrace{U\mathrm{Re}[\psi^*_{k,l}(\partial\nabla^2\tau/\partial x)_{k,l}]}_{\mathrm{III}}$$

$$+ \underbrace{\kappa\,\mathrm{Re}[\psi^*_{k,l}(\nabla^2(\psi - \tau)/2)_{k,l}]}_{\mathrm{IV}} + \underbrace{\nu\,\mathrm{Re}[\psi^*_{k,l}(\nabla^8(\nabla^2\psi))_{k,l}]}_{\mathrm{V}}, \quad (5a)$$

$$\partial[(k^2 + l^2 + k_d^2)|\tau_{k,l}|^2/2]/\partial t = \underbrace{\mathrm{Re}[\tau^*_{k,l}J_{k,l}(\tau, \nabla^2\psi)]}_{\mathrm{I}} + \underbrace{\mathrm{Re}[\tau^*_{k,l}J_{k,l}(\psi, \nabla^2\tau)]}_{\mathrm{II}}$$
$$+ \underbrace{\mathrm{Re}[\tau^*_{k,l}J_{k,l}(\psi, -k_d^2\tau)]}_{\mathrm{III}} + \underbrace{U\,\mathrm{Re}[\tau^*_{k,l}(\partial\nabla^2\psi/\partial x)_{x,l}]}_{\mathrm{IV}} + \underbrace{Uk_d^2\,\mathrm{Re}[\tau^*_{k,l}(\partial\psi/\partial x)_{k,l}]}_{\mathrm{V}}$$
$$+ \underbrace{\kappa\,\mathrm{Re}[\tau^*_{k,l}(\nabla^2(\tau - \psi)/2)_{k,l}]}_{\mathrm{VI}} + \underbrace{\nu\,\mathrm{Re}[\tau^*_{k,l}(\nabla^8(\nabla^2\tau - k_d^2\tau))_{k,l}]}_{\mathrm{VII}}, \quad (5b)$$

where $(\ldots)_{k,l}$ refers to the 2D Fourier transform of an expression and $(\ldots)^*$ the complex conjugate. Note that the "linear" terms III in (5a) and IV in (5b) cancel each other, wavenumber by wavenumber, leaving V in (5b) as a sole source of energy for the system. The nonlinear counterparts of the modal energy exchange terms, II in (5a) and II in (5b), cancel when summed over wavenumber, but one should keep in mind that the source of barotropic energy due to this nonlinear exchange does not have, in general, the same spectral shape as the corresponding sink of energy in the baroclinic mode.

Figure 4 presents a set of spectral characteristics of the flow at equilibrium. All are time averaged over the 150 time unit period shown in Fig. 2. Although Fig. 2a shows a small trend in the barotropic energy, the averaged barotropic energy budget balances to within a fraction of a percent (see Table 1), and experimentation with other versions of the model show that its qualitative behavior is robust. The energy spectra (Fig. 4a) indicate a dominance of the barotropic energy over the total (kinetic plus potential) baroclinic energy for scales larger than the deformation radius. (The baroclinic energy on these scales is almost entirely potential.) On scales smaller than the deformation radius, the baroclinic energy dominates. The slopes are close to a $-5/3$ power law in the range $k \in [2, \sim 10]$, with the barotropic slope slightly steeper and the baroclinic one slightly less steep, although the statistics for the largest scales are not very robust due to the long intrinsic timescales of these eddies.

The baroclinic energy transfers (Fig. 4c) are dominated by two terms: the linear production (V) and the energy transfer due to the advection of thickness by the *barotropic* velocity field (III). Energy is injected only at the largest scales $k \in [1, \sim 3]$ and removed from these scales by the barotropic advection. The energetic contributions of the two terms $J(\tau, \nabla^2\psi)$ (I) and $J(\psi, \nabla^2\tau)$ (II) are of approximately equal amplitude and opposite in sign for k less than ~ 15. Since term II transfers baroclinic energy to the barotropic mode while I only redistributes baroclinic energy between different scales, the cancellation has the effect that the transfer out of the baroclinic mode is concentrated toward the scale of the deformation radius. As a result, there is an extended approximate inertial range, with invariant downscale baroclinic energy flux, for $k \in [\sim 3, \sim 15]$, as shown in Fig. 4d.

The energy transfers for the barotropic mode (Fig. 4b) show the familiar 2D inverse energy cascade to larger scales, resulting from the term $J(\psi, \nabla^2\psi)$. The linear term is negligible. A surprising feature is that the nonlinear energy influx from the baroclinic mode is spread almost uniformly over the range $k \in [1, \sim 15]$, in contrast to the outflux from the baroclinic mode, which is concentrated at smaller scales. As a consequence, the barotropic mode does not show a clear inertial range with constant upscale energy transfer (see Fig. 4d).

In the baroclinic mode, the direct effect of dissipation on the energetics is very small. In the barotropic mode, the energy that cascades toward larger scales is damped by the Ekman friction. The energy transfer rates and the energies averaged over space and time are summarized in Table 1, where this calculation is referred to as case I.

The kinetic energy spectra in the u and v components are shown in Fig. 4e. The baroclinic kinetic energy peaks at $k \sim 25$, exceeding its value at $k = 1$ by a factor of 5. The only anisotropy evident is on the largest scales in the baroclinic mode. The remarkable isotropy for all but the largest scales is also shown by the correlation coefficient (Fig. 4f) between the interface height τ and barotropic velocity v_ψ. This confinement of the correlation to large scales and the growth of both barotropic energy and baroclinic potential energy toward smaller k combine to sharply localize the energy production at the largest scales.

Enstrophy spectra and enstrophy transfer spectra (not shown) show baroclinic enstrophy being generated on large scales, flowing toward the deformation scale where there is transfer to the barotropic mode, and then continuing to flow toward small scales in roughly equal proportions in the two modes.

The picture suggested by this calculation is that the baroclinic production occurs on the largest scale to which the inverse barotropic cascade extends or the scale of the large-scale baroclinicity, whichever is smaller. (In the present homogeneous calculation, the baroclinicity covers the entire domain.) To examine this point further, one could add the beta effect, which would arrest the cascade but introduce the added complication of strong anisotropy and jet formation. Here,

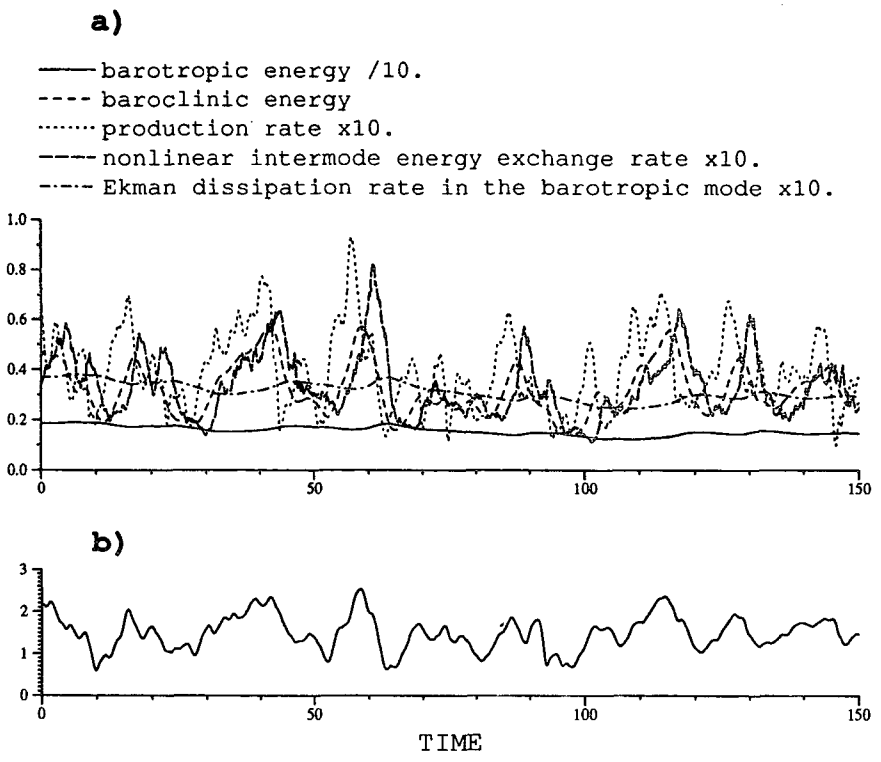

FIG. 2. (a) Time series of area averaged modal energies and energy transfer rates. The production rate is term V in (5b); the nonlinear intermode energy exchange rate is term II in (5a) (which is also equal to the negative of term II in (5b); and the barotropic Ekman dissipation rate is IV in (5a). (b) The ratio of the amplitude of the $k = 1$ harmonic in the meridional velocity to the mean current velocity U.

we choose the simpler alternative of controlling the scale of the production directly, artificially modifying the linear terms in (4) so that they are identically zero for $|k| \leq k_c$. One expects the production to peak at wavenumbers slightly larger than k_c. The inverse barotropic cascade, if sufficiently energetic, is still able to proceed toward the basin scale (the domain size). Here we describe a calculation with $k_c = 4$, with all other parameters unchanged. In the following, this experiment is referred to as case II.

The energy level reached by this flow is much smaller than in I. The production and barotropic energy are both approximately 60 times smaller, while the total baroclinic energy and the baroclinic kinetic energy are a factor of 30 and 15 smaller, respectively. These values are tabulated in Table 1. Some spectra for case II are shown in Fig. 5. The production is now localized in $k \in [5, 10]$. Qualitatively, the energy transfers are unchanged, although there is not enough room for a clear inertial range in the cascade of baroclinic energy downscale in this case. Also, because of the reduced energy level and the longer eddy turnover times, the inverse barotropic cascade does not reach the domain scale before being dissipated through Ekman friction. As shown by the domain-averaged energy integrals in Table 1 the linear term plays a somewhat more important role in the barotropic mode due to the smaller eddy amplitudes. The equipartition of kinetic energy between u and v remains very clear, with anisotropy visible only on the scales at which the production occurs.

It is a coincidence that the barotropic cascade stops near k_c in this integration. An additional integration has been performed with the Ekman friction coefficient reduced from 0.04 to 0.015. The resulting energy spectra have been included in Fig. 5a. The barotropic spectrum extends to larger scales with the peak at $k = 1$ and 2, but the baroclinic energy spectrum's shape and amplitude remain almost the same. The total baroclinic energy actually decreases by 11% and the production rate by 12%, while the barotropic energy increased by 120%. Therefore, to first approximation, the energy production is controlled by the energy of the eddies near the scale k_c and not by the more energetic eddies on larger scales. The opposite situation, in which the inverse cascade stops before reaching k_c occurs in the beta-plane simulations to be described elsewhere. The results are consistent with the simple picture outlined above, in which the energy production is controlled by the scales to which the inverse cascade extends, or the

largest scales on which there is available potential energy to be tapped, whichever is the smaller.

Two additional experiments with the parameters as in case I, but with larger Ekman damping rates, are also described in Table 1. These are motivated by the following scaling analysis.

4. Theory

A conceptually simple picture of energy transformations in the two-layer model was advanced by Rhines (1977), Salmon (1978, 1980), and Hoyer and Sadourny (1982) that is consistent with these model calculations. In this picture, the baroclinic energy injected at large scales cascades down to the deformation radius, where it is converted to the barotropic mode and then proceeds to cascade upscale.

As we have seen, the dynamics of the barotropic mode is dominated by barotropic self-advection, large-scale dissipation, and the forcing, mostly nonlinear, by the baroclinic component of the flow. If the latter were localized at scales near k_d, one would have the classical formulation of a problem that would generate an inverse energy cascade. Although the forcing is not, in fact, well localized, we will proceed with this simple picture, discussing corrections afterward. For the barotropic energy spectrum, E_ψ, a $-5/3$ power law is expected (Kraichnan 1967; Leith 1968; Batchelor 1969):

$$E_\psi = C_\psi \epsilon_\psi^{2/3} k^{-5/3} \tag{6}$$

(ϵ_ψ is the barotropic kinetic energy cascade rate and C_ψ a universal constant).

As Salmon (1980) notes, the nonlinear dynamics of the baroclinic mode in the limit of large scales ($k^2 \ll k_d^2$) reduces to 2D advection of a passive scalar by the barotropic flow:

$$\partial\tau/\partial t + J(\psi, \tau) = 0. \tag{7}$$

We are ignoring for the moment the mean potential vorticity gradient associated with the vertical shear. The form of the scalar variance spectrum and the direction of its cascade, given the inverse cascade of the kinetic energy for the ψ field, is discussed by Lesieur and Herring (1985). Studies of closure models for (7) (Lesieur and Herring 1985; Hoyer and Sadourny 1982) show that the cascade of the scalar variance is direct with a $-5/3$ power law spectrum; however, correlations between the scalar and the vorticity of the advecting field may change the slope (Lesieur and Herring, 1985). We are not aware of any direct numerical simulations that focus on the large-scale tracer transport with a statistically stationary inverse energy cascade in the advecting field [other studies which consider the direct enstrophy cascade, decaying 2D turbulence, β-plane, etc. may be found in Holloway and Kristmannsson (1984), Babiano et al. (1987), and Bartello and Holloway (1991)].

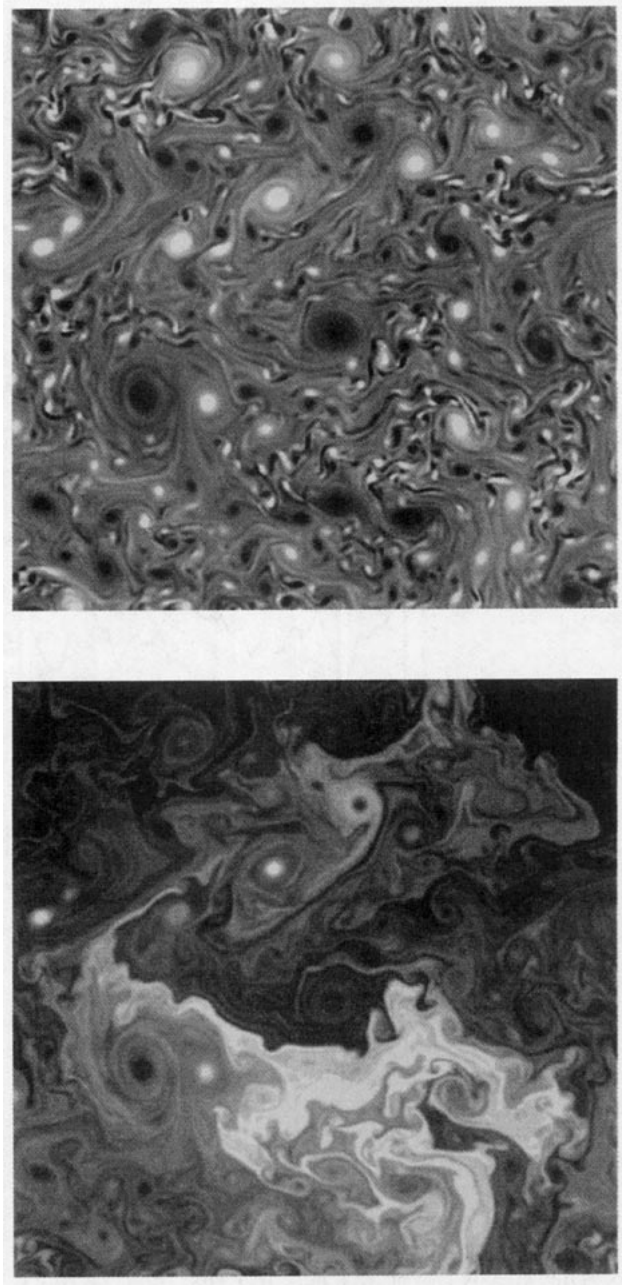

FIG. 3. Barotropic (upper panel) and baroclinic (lower panel) potential vorticity fields at $t = 17.5$. (The gray scales are the same in the two panels except that the baroclinic potential vorticity has been divided by 4.0.)

We use the symbol ϵ_τ for the cascade rate of the baroclinic energy, which equals k_d^2 times the cascade rate for $\langle\tau^2\rangle$ on large scales. Relying on the classical phenomenological argument based on spectral locality, we assume that

$$\epsilon_\tau = \text{const} \sim (E_\tau k)/T_k,$$

where T_k is the typical eddy lifetime. Since the latter is determined only by the advective field ψ, dimensional

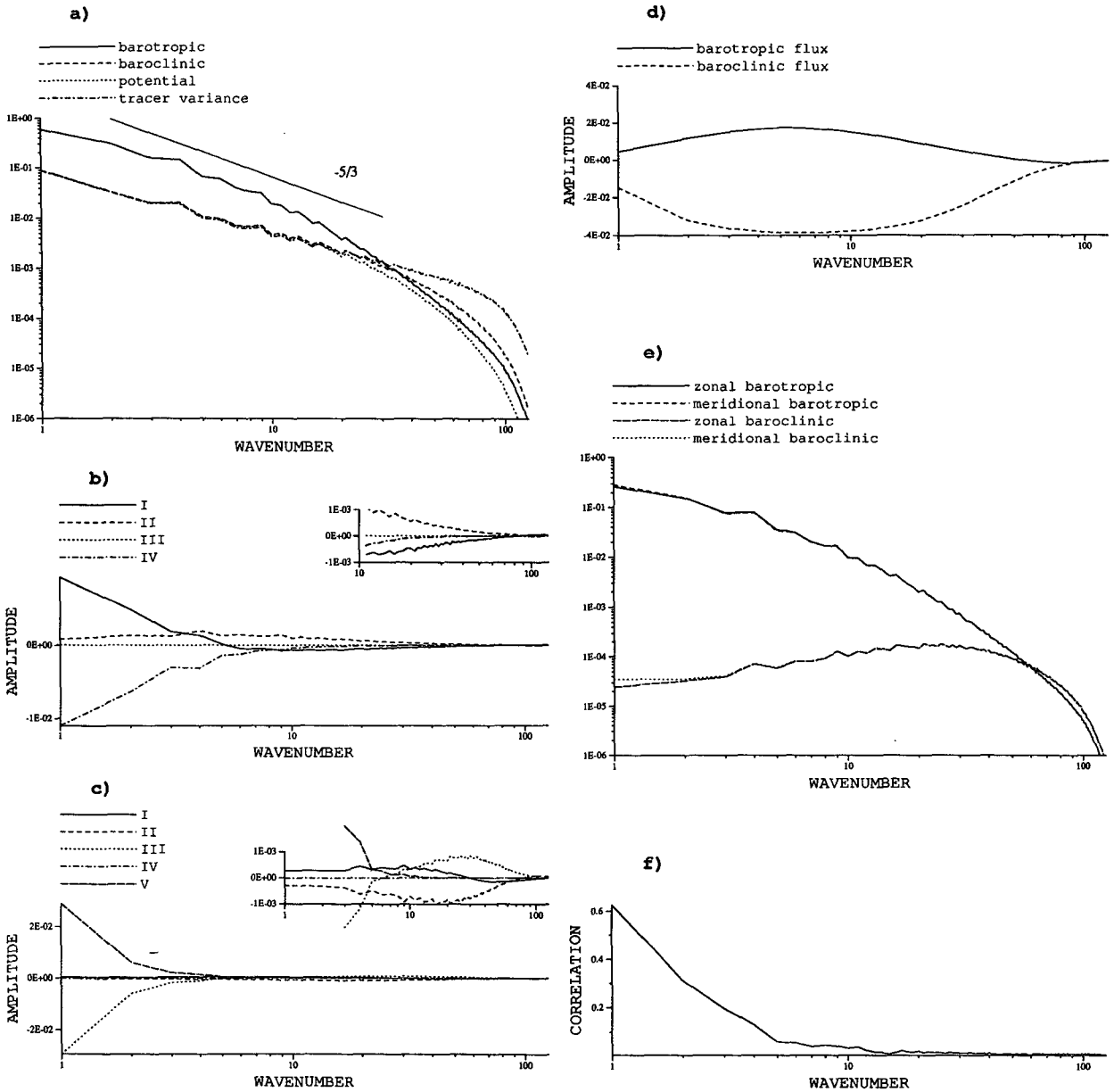

FIG. 4. Spectral energetics for case I: (a) barotropic, baroclinic, and potential energy spectra, and passive tracer variance spectrum; (b) the energy transfer rates in the barotropic mode due to different terms in Eq. (5a) (detailed structure is shown in inserts; if terms are not plotted, they have negligible amplitude); (c) energy transfer rates in the baroclinic mode due to different terms in Eq. (5b); (d) the upscale energy flux in the barotropic mode and the downscale energy flux in the baroclinic mode, obtained by integrating term I in Eq. (5a) and term III in Eq. (5b), respectively; (e) the spectra of the kinetic energy in zonal and meridional flow for barotropic and baroclinic modes; and (f) the correlation coefficient between τ and the barotropic meridional velocity v_ψ averaged over angle in wavenumber space.

considerations and the locality assumption give $T_k \sim (E_\psi k^3)^{-1/2}$, which together with (6) yields

$$E_\tau = C_\tau \epsilon_\tau \epsilon_\psi^{-1/3} k^{-5/3}. \quad (8)$$

While our model is still far from the asymptotic limit in which this passive scalar model is valid over a wide range of scales, the tendency for the energy transfers associated with the terms $J(\tau, \nabla^2\psi)$ and $J(\psi, \nabla^2\tau)$ to nearly cancel each other at intermediate values of k extends the inertial range closer to $k \sim k_d$ than would otherwise be the case.

The picture of the looping energy path in the model implies that the cascade rate of the baroclinic energy to smaller scales is equal to the cascade rate back to larger scales in the barotropic mode:

TABLE 1. Values of model parameters and domain-averaged energetics in the four statistically steady states described in the text.

Parameter/energetics	Experiment/case I	II	III	IV
k_d	50	50	50	50
$2U$	0.01	0.01	0.01	0.01
κ	0.04	0.04	0.08	0.25
ν	$0.512\cdot10^{-15}$	$0.512\cdot10^{-15}$	$0.512\cdot10^{-15}$	$0.512\cdot10^{-15}$
k_c	0	4	0	0
E_τ	0.323	$0.102\cdot10^{-1}$	$0.239\cdot10^{-1}$	$0.117\cdot10^{-2}$
$\langle u_\psi^2\rangle$	0.779	$0.126\cdot10^{-1}$	$0.135\cdot10^{-1}$	$0.218\cdot10^{-3}$
$\langle v_\psi^2\rangle$	0.798	$0.123\cdot10^{-1}$	$0.138\cdot10^{-1}$	$0.227\cdot10^{-3}$
$\langle u_\tau^2\rangle$	$0.833\cdot10^{-2}$	$0.569\cdot10^{-3}$	$0.970\cdot10^{-3}$	$0.103\cdot10^{-3}$
$\langle v_\tau^2\rangle$	$0.832\cdot10^{-2}$	$0.569\cdot10^{-3}$	$0.965\cdot10^{-3}$	$0.109\cdot10^{-3}$
E_ψ/E	0.830	0.709	0.533	0.276
$\langle\psi J(\tau, \nabla^2\tau)\rangle$	$0.338\cdot10^{-1}$	$0.521\cdot10^{-3}$	$0.113\cdot10^{-2}$	$0.258\cdot10^{-4}$
$\langle U\cdot\psi\partial\nabla^2\tau/\partial x\rangle$	$0.115\cdot10^{-3}$	$0.298\cdot10^{-4}$	$0.359\cdot10^{-4}$	$0.107\cdot10^{-4}$
$\langle\kappa\cdot\psi\nabla^2(\psi-\tau)/2\rangle$	$-0.314\cdot10^{-1}$	$-0.485\cdot10^{-3}$	$-0.103\cdot10^{-2}$	$-0.322\cdot10^{-4}$
$\langle\nu\cdot\psi\nabla^8(\nabla^2\psi)\rangle$	$-0.266\cdot10^{-2}$	$-0.583\cdot10^{-4}$	$-0.117\cdot10^{-3}$	$-0.397\cdot10^{-5}$
$\langle U\cdot k_d^2\cdot\tau\partial\psi/\partial x\rangle$	$0.396\cdot10^{-1}$	$0.696\cdot10^{-3}$	$0.144\cdot10^{-2}$	$0.474\cdot10^{-4}$
$\langle\kappa\cdot\tau\nabla^2(\tau-\psi)/2\rangle$	$-0.177\cdot10^{-3}$	$-0.105\cdot10^{-4}$	$-0.182\cdot10^{-4}$	$-0.297\cdot10^{-5}$
$\langle\nu\cdot\tau\nabla^8(\nabla^2\tau-k_d^2\tau)\rangle$	$-0.517\cdot10^{-2}$	$-0.124\cdot10^{-3}$	$-0.233\cdot10^{-3}$	$-0.789\cdot10^{-5}$

$$\epsilon_\psi = \epsilon_\tau. \tag{9}$$

As seen in Fig. 4d, this is not a good quantitative fit to the model results, partly because there is no clean inertial range in the barotropic mode due to the distributed nonlinear source and partly because some of the energy has been dissipated on small scales as the energy passes through this loop. Accepting (9) as a qualitative guide, one has (as in Hoyer and Sadourny 1982)

$$E_\psi = C_\psi\epsilon_\tau^{2/3}k^{-5/3} \tag{10a}$$

$$E_\tau = C_\tau\epsilon_\tau^{2/3}k^{-5/3}, \tag{10b}$$

suggesting that the ratio $E_\psi/E_\tau = C_\psi/C_\tau$ is invariant in the inertial range and independent of ϵ_τ and k_d. Therefore, we have the scaling relation

$$\psi_k \sim (k_d/k)\tau_k \tag{11a}$$

for $k^2 \ll k_d^2$. Note also that the baroclinic kinetic energy spectrum $E_{\tau\text{kin}} = (k/k_d)^2E_\tau$ grows slowly toward smaller scales, like $k^{1/3}$, as Figs. 4e and 5e corroborate.

Since the spectra in (10) are steeper than k^{-1}, energetically the ψ and τ fields are both dominated by the largest scales to which these spectra extend. Denoting this largest energy-containing scale as k_0, the relation between the magnitudes of the *physical space* barotropic and baroclinic eddy streamfunctions is therefore

$$\psi \sim (k_d/k_0)\tau. \tag{11b}$$

From an eddy-damped quasi-normal Markovian theory, Lesieur and Herring (1985) estimate $C_\tau = 0.29$, given the value $C_\psi = 6.69$ suggested by Kraichnan (1971). [Note that a recent direct numerical high-resolution simulation of 2D flow finds $C_\psi = 5.58$ (Maltrud and Vallis 1991).] Despite misgivings about the accuracy of the closure estimate and the extent to which our results are in the asymptotic limit, the qualitative results are consistent: the barotropic energy is larger by a substantial amount. The same amount of energy is cascading up the barotropic spectrum as is cascading down the baroclinic spectrum in this picture, but the former is much less efficient and requires larger energies to produce the same energy flux.

If we attempt to estimate C_τ and C_ψ by fitting the model results to $-5/3$ spectra, we find $C_\psi = 5.1$, $C_\tau = 0.79$ for case I, and $C_\psi = 4.1$, $C_\tau = 1.1$ for case II. (To obtain these estimates, we set ϵ_τ equal to the rate of production of baroclinic energy, and we take ϵ_ψ equal to the rate of dissipation of barotropic energy by Ekman friction, which is slightly smaller in the numerical model.) Considering the inadequate resolution of the inertial ranges in the model, and the steeper barotropic spectrum, the discrepancy with the estimates given above is not unreasonable. The smaller ratio C_ψ/C_τ in case II implies a smaller ratio of energies E_ψ/E_τ. As noted earlier, the barotropic energy increases by a factor of 60 from cases II to I, while the baroclinic energy increases only by a factor of 30. Therefore, (11) provides only a rough guide to the model's behavior.

The steeper barotropic spectrum may be related to the broadly distributed energy input from the baroclinic mode. As one moves to smaller k, ϵ_ψ increases due to this distributed energy input. Assuming that we can still use (6) locally in k space, this implies a steeper barotropic spectrum and, from (8), a less steep baroclinic spectrum. One would therefore expect the ratio E_ψ/E_τ to be larger in case I than in case II since the difference between the slopes extends for a larger range of wavenumbers in the former case. By fitting a simple function

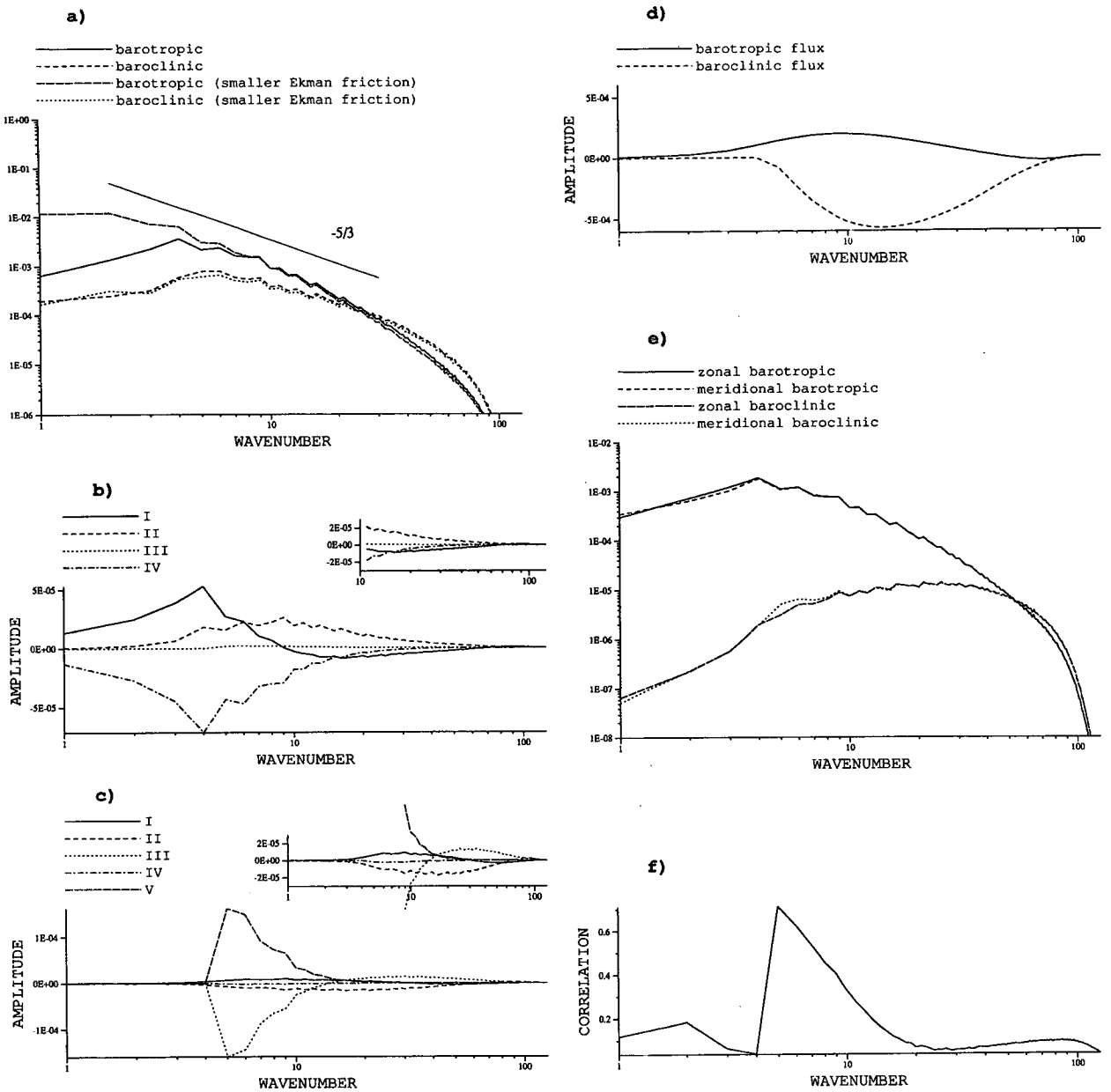

FIG. 5. Spectral energetics for case II. As in Fig. 4 except that (a) also shows the energy spectra for the experiment with smaller Ekman friction.

to the shape of $\epsilon_\psi(k)$, one can try to make this argument more quantitative, but we do not pursue this point here.

The production of baroclinic energy is proportional to the northward transport of thickness (or heat):

$$\epsilon_\tau = Uk_d^2\langle \tau v_\psi \rangle. \tag{12}$$

The potential vorticity fluxes are also proportional to the thickness flux in this homogeneous system:

$$\langle v_i q_i \rangle = (-1)^i k_d^2 \langle \tau v_\psi \rangle. \tag{13}$$

We can also write

$$\langle \tau v_\psi \rangle = \int c(\tau, v_\psi)(E_\tau E_\psi)^{1/2} dk, \tag{14}$$

where $c(\tau, v_\psi)$ is the correlation coefficient. Even if the correlation had no structure in k, given (10) the multiplier $(E_\tau E_\psi)^{1/2}$ alone would make the integral divergent at small k, implying that most of the contribution to the heat or potential vorticity transport would come from the largest scales. That the correlation is high only

on the largest scales makes these scales even more dominant.

To estimate the production of baroclinic energy ϵ_τ, we reintroduce the environmental thickness gradient into (7):

$$\partial\tau/\partial t + J(\psi, \tau - Uy) = 0. \tag{15}$$

In this approximation, the problem of computing the energy production is equivalent to computing the flux of the conserved tracer τ in the presence of a linear large-scale gradient, due to advection by a prescribed field ψ—the classical problem of turbulent diffusion. Standard mixing arguments suggest that the typical magnitude of the physical space perturbations in τ on the scale k_0 of the energy-containing eddies will be

$$\tau \sim U/k_0 \quad \text{or} \quad v_\tau \sim U. \tag{16a}$$

In terms of the spectral amplitudes at this scale, we have instead

$$\tau_k \sim Uk_0^{-3/2} \quad \text{at} \quad k = k_0. \tag{16b}$$

In experiment I, an appropriate choice would be $k_0 \sim 1$; in experiment II, $k_0 \sim 5$–6.

In Fig. 2b, the magnitude of the baroclinic velocity at $k = 1$ is plotted as a function of time for case I. This plot shows the approximate validity of (16) for the statistically steady state (in the time mean, $v_\tau/U = 1.6$) and also gives one some feeling for the close dynamical relation between the production and v_τ. In case II, if we consider only the variance in $k = 5$, we find $v_\tau/U = 1.2$ in the time mean. If we include the variance in $k = 6$ as well, then this ratio is increased to 2.0. The poor resolution due to discreteness of the spectral domain on these scales makes it difficult to be more precise, but given the large changes between I and II in the production and the total energy levels, the claim that the *baroclinic* velocities on the largest scales contributing to the flux are of the same magnitude as U is qualitatively supported.

Combined with (10), the relation (16) determines the spectra of the barotropic and baroclinic modes. Using the relation (11), (10) implies the physical space amplitudes

$$\tau \sim k_0^{-1}U \quad \text{and} \quad \psi \sim (k_d/k_0^2)U \tag{17a}$$

or, in terms of spectral amplitudes,

$$\tau_k \sim k_0^{-3/2}U \quad \text{and} \quad \psi_k \sim (k_d/k_0^{5/2})U \quad \text{at} \quad k = k_0. \tag{17b}$$

Therefore, the production scales as

$$\epsilon_\tau \sim Uk_d^2 k_0 \psi\tau \sim U^3k_d^3/k_0^2. \tag{18}$$

To obtain this scaling in a slightly different way, assume that the correlation between τ and v_ψ is perfect between k_0 and $k_0 + \Delta k$, and zero otherwise, so that

$$\epsilon_\tau = Uk_d^2\langle\tau v_\psi\rangle = Uk_d\int_{k_0}^{k_0+\Delta k}(E_\tau E_\psi)^{1/2}dk.$$

Alternatively, we can think of this expression as defining Δk. Using (10), we then have

$$\epsilon_\tau = \frac{3}{2}Uk_d(C_\psi C_\tau)^{1/2}\epsilon_\tau^{2/3}k_0^{-2/3} \times (1 - [(k_0 + \Delta k)/k_0]^{-2/3}).$$

Solving for ϵ_τ and assuming that $\Delta k \sim k_0$, we retrieve (18). The assumption that $\Delta k \sim k_0$ is consistent with the picture of the correlation as being determined by Eq. (15), in which there is no other length scale.

The dependence $\epsilon_\tau \sim k_0^{-2}$ is roughly consistent with the numerical experiments: the ratio of the energy production in cases I and II (see Table 1) is 57, while $k_0 \sim 1$ for I and ~5–6 for II. Note also that the range of k for which the correlations are significant (Δk above) is roughly proportional to k_0 (Figs. 4f and 5f).

These correlations drop to remarkably small values well before the deformation scale is reached, especially in Fig. 4f. We can try to understand the negligible transport and energy production by deformation-scale eddies in the context of the baroclinic energy cascade. An eddy of scale k does not simply feel the environmental baroclinic potential vorticity gradient directly, but instead feels the gradient as modified by all larger eddies in the cascade (see Fig. 3). To the extent that the baroclinic cascade is able to isotropize the gradient as seen by a given scale, eddies on that scale will not, on average, be able to transport potential vorticity or produce eddy energy.

The scaling (17) implies that the timescale T_0 of the energy-containing barotropic eddies with wavenumber k_0 is

$$T_0 \sim (E_\psi k_0^3)^{-1/2} \sim 1/(k_0^{5/2}\psi_k) \sim 1/(k_dU), \tag{19}$$

which is independent of k_0. This is also the characteristic timescale of the linear baroclinic instability near k_d. This scaling has interesting implications for the role of Ekman friction in this model. If the energy level of the flow were fixed, then the timescale of the energy-containing eddies would increase as energy cascaded to larger scales, and Ekman friction would eventually grow to $O(1)$ importance and stop the cascade. But with the present scaling, the energy level increases as the scale k_0^{-1} increases and in such a way that the timescale of the energy-containing eddies does not increase. Therefore, if $\kappa \ll k_dU$, the Ekman damping will never be able to halt the cascade. On the other hand, if $\kappa \geq k_dU$, the Ekman friction will be of $O(1)$ importance at the deformation radius, so one does not expect a significant inverse cascade of barotropic energy. (In this case the damping also has a significant effect on the linear baroclinic instability.) The implication is that there should be a dramatic decrease in eddy energy at some point as κ is increased significantly over k_dU.

Haidvogel and Held (1980, Fig. 14) provide results for experiments with $\kappa/(k_d \cdot 2U) = 0.35$ and 0.5, for which the total eddy energy levels, normalized by $(2U)^2$, are 17.7 and 9.0, respectively. In our experiment, $\kappa/(k_d \cdot 2U) = 0.08$, and the energy level normalized in the same way is 9.5×10^3! To make contact with the parameter range of Haidvogel and Held, we have performed two additional experiments with larger Ekman damping (cases III and IV in Table 1). For $\kappa/(k_d \cdot 2U) = 0.16$, and 0.5, we obtain normalized energies of 256, and 8.0, the latter value being consistent with Haidvogel and Held (1980). The sensitivity to damping in this model is indeed exceptionally strong, consistent with our scaling argument.

In order to check on the consistency of our explanation for the energy generation and heat flux in this system, we have performed several supplementary calculations. In particular, a passive tracer was added to the model and simply advected by the barotropic flow produced in case I. The equation solved is (15) with ∇^8 diffusion added. The tracer and thickness equations differ only due to the $O(k/k_d)^2$ terms in the latter. The tracer was initialized with small random values. The resulting tracer variance spectrum has been included in Fig. 4a. Not only is this variance almost identical to that of the thickness on large scales, but the tracer flux (not shown) is nearly identical to the thickness flux. In fact, the correlation coefficient between the tracer and τ is nearly perfect on large scales, decreasing from 1.0 at $k = 1$ to 0.9 near $k = 30$. Therefore, the structure of the baroclinic mode on large scales can be studied in the framework of passive tracer 2D advection. Conversely, it follows that the transport of passive tracer in such a model is dominated by the largest scales.

We have also performed computations in which the barotropic energy is maintained at a much higher level than would naturally occur in this system, by holding constant the Fourier harmonics for the barotropic mode in the wavenumber range [30, 40]. This removes the feedback from the baroclinic onto the barotropic mode and makes the barotropic forcing more localized in wavenumber. The spectral slopes of the baroclinic and barotropic energies are now closer to each other, and both are closer to $-5/3$, so it does appear that the nonlocal source of barotropic energy that occurs in the full system steepens the barotropic and flattens the baroclinic spectra slightly. One still sees cancellation in the baroclinic mode energetics between the terms resulting from $J(\psi, \nabla^2\tau)$ and $J(\tau, \nabla^2\psi)$ in the range $k \in [1, 12]$, which again has the effect of localizing the energy lost from the baroclinic mode to scales near k_d.

5. Discussion and conclusions

We have studied the horizontally homogeneous, statistically steady state of a baroclinically unstable, two-layer, quasigeostrophic fluid under conditions that result in an inverse energy cascade to scales much larger than the deformation radius. The instability is generated by a uniform vertical shear in the mean current, or thickness gradient, $U = -\partial\tau/\partial y$. The following picture emerges as a simple way of understanding the energy levels and the magnitude of the fluxes in this system.

The central point is that the *energy production and the associated potential vorticity fluxes are localized at the largest scales to which both the barotropic inverse energy cascade and the baroclinicity of the mean flow extend,* and not at the deformation scale.

As discussed by Rhines (1977) and Salmon (1978, 1980), on large scales the eddies are almost entirely barotropic, and the dynamics of the baroclinic mode reduces to the advection of the thickness τ, or large-scale potential vorticity, by this barotropic flow ψ. Given the existence of the mean gradient, the flux of thickness down this gradient can be thought of as produced by the turbulent diffusion generated by the flow field ψ. Since the largest-scale eddies to which the inverse barotropic cascade extends are also the most energetic, we must expect these eddies to dominate the flux.

One can estimate this flux by assuming a diffusivity $D = V\Lambda$, where the mixing length $\Lambda = k_0^{-1}$ is the scale of the energy-containing eddies, and the velocity scale V is the characteristic barotropic flow speed. The characteristic size of the perturbations in thickness on the scale of k_0 is expected to be Uk_0^{-1} based on the passive tracer analogy. The eddy heat and potential vorticity fluxes, and the baroclinic eddy energy generation are all proportional to this thickness flux. Estimating these quantities requires an estimate of the barotropic energy level and the energy-containing scale k_0^{-1}.

Given the equality of the rates at which the energy cascades to small scales in the baroclinic mode and cascades upscale in the barotropic mode, the phenomenological inertial range theory implies that the barotropic and baroclinic energy levels should be comparable. (Another way of arguing this is to note that the ratio E_ψ/E_τ may depend only on the cascade rate ϵ_τ and k, which do not make a nondimensional quantity.) In terms of spectral amplitudes we have $\psi_k \sim (k_d/k)\tau_k$. Since the spectra are such that the largest scales dominate the variances of ψ and τ, the physical space rms amplitudes satisfy $\psi \sim (k_d/k_0)\tau$, where k_0 is the energy-containing scale. Therefore, the characteristic barotropic speed V to be used in estimating the thickness flux is $k_0\psi \sim k_d\tau$, or Uk_d/k_0.

The resulting diffusivity has the magnitude Uk_d/k_0^2. This should be compared to the diffusivities implicit in the discussions of atmospheric eddy fluxes in Stone (1972) and Green (1970). Stone assumes that the mixing length is the radius of deformation and that the typical eddy velocity is of the order of the mean shear U, resulting in a diffusivity that scales as U/k_d. This is equivalent to assuming that eddy kinetic and eddy available potential energies are comparable and that

each is of the order of the mean available potential energy contained within a region of width equal to the deformation radius. Green also effectively assumes equipartition of eddy kinetic and eddy available potential energies but assumes that these are of the order of the available potential energy in the entire baroclinic zone. If the width of this zone is k_0^{-1}, this leads to the same diffusivity as we have obtained, Uk_d/k_0^2. We emphasize, however, that it is only if the inverse energy cascade reaches the scale of the baroclinic zone that we can set k_0 equal to that scale. If the cascade stops earlier, due to the beta-effect for example, k_0 will be set by this smaller scale. Implications of this scaling for eddy fluxes and the scale of eddy-driven jets on a beta plane will be discussed elsewhere. Also, our explanation for approximate equipartition of eddy kinetic and potential energies is quite different from that usually considered in such scaling arguments. More typically, as in Stone (1972), one assumes that deformation-scale eddies are of central importance, and one automatically has equipartition on this scale between the kinetic and potential energies in the *baroclinic* mode. Barotropic velocities are implicitly assumed to be of the same order as the baroclinic velocities, as is typically true in the most unstable linear modes, for example. In the case of an extensive inverse cascade on which we focus here, the kinetic energy is almost entirely barotropic, but the arguments leading to (11) still imply approximate equipartition between this kinetic energy and the potential energy in the baroclinic mode.

This zeroth-order picture must be modified in several ways to account quantitatively for our numerical results. First, the direct cascade of baroclinic energy is much more efficient than the inverse barotropic cascade, in that the same spectral energy flux is produced with a smaller energy level. The barotropic energies are an order of magnitude larger as a result. Second, the transfer of energy to the barotropic mode is not sharply localized at the scale of the deformation radius; the source actually extends to very large scales. This has the effect of steepening the barotropic energy spectrum and flattening the baroclinic spectrum. Third, the loss of energy from the baroclinic mode is more sharply confined to the deformation scale, but only because of a cancellation of terms in the energetics the reasons for which we do not understand. These quantitative aspects of our results may be sensitive to the particular model that we have studied. However, we believe that the zeroth-order scaling will be robust within the framework of quasigeostrophic theory.

Since this analysis is based on a quasigeostrophic model, it is suspect on scales much larger than the deformation radius unless the Rossby number is extremely small. In more general models, the possibility exists that baroclinic large-scale coherent eddies could dramatically alter the vertical structure of the eddy velocity field.

The role played by deformation-scale eddies in our calculation is strikingly modest. The potential vorticity flux and energy generation on these scales is totally negligible, although there is a weak maximum in the baroclinic *kinetic* energy spectrum, and the loss of baroclinic energy to the barotropic mode does occur on this scale. That the eddy energy moves to larger scales as the flow becomes more strongly unstable is a familiar idea. That the generation itself moves to larger scales is less familiar but has often been observed in numerical models. The large separation in our calculation between the deformation radius and the size of the domain (and the absence of the β-effect, which allows the cascade to reach the domain scale) makes this movement very clear. In this regime, linear growth rates on the mean shear play no direct role in the closure. A good indicator of this is the negligible role played by the linear term in the barotropic energetics. Instead, the mean shear provides a thickness gradient that supports the diffusive flux generated by the barotropic flow; the barotropic flow, in turn, is supported by the energy generation associated with the downgradient thickness flux.

Any attempt at using these concepts to estimate oceanic diffusivities due to baroclinic instability will revolve around estimating the scale to which the inverse energy cascade extends. If one can think of the cascade as being halted by the beta effect, this estimate should be relatively straightforward. If one needs to consider the inhomogeneous system in order to understand how the cascade is halted—if, for example, the radiation of coherent vortices away from an unstable region is an essential ingredient—this will be much more difficult.

Acknowledgments. A need to reassess the theory of strongly nonlinear baroclinic instability to comprehend fluxes and transports in the ocean surfaced during long, stimulating discussions between Jim McWilliams, Geoff Vallis, and the first author (VL) at UCSC in spring–summer of 1991. The hospitality of the university and Dr. G. Vallis is gratefully acknowledged. Ron Pacanowski kindly provided us with assistance in graphics. We also thank two reviewers for helpful comments. This paper is funded by a grant/cooperative agreement from the National Oceanic and Atmospheric Administration (Grant NA26RG0102-01). The views expressed herein are those of the authors and do not necessarily reflect the views of NOAA or any of its subagencies.

REFERENCES

Babiano, A., C. Basdevant, B. Legras, and R. Sadourny, 1987: Vorticity and passive-scalar dynamics in two-dimensional turbulence. *J. Fluid Mech.*, **183**, 379–397.

Bartello, P., and G. Holloway, 1991: Passive scalar transport in β-plane turbulence. *J. Fluid Mech.*, **223**, 521–536.

Batchelor, G. K., 1969: Computation of the energy spectrum in two-dimensional turbulence. *Phys. Fluids* (Suppl.), **12**(II), 233–239.

Green, J. S. A., 1970: Transfer properties of the large-scale eddies and the general circulation of the atmosphere. *Quart. J. Roy. Meteor. Soc.*, **96,** 157–185.

Haidvogel, D. B., and I. M. Held, 1980: Homogeneous quasi-geostrophic turbulence driven by a uniform temperature gradient. *J. Atmos. Sci.*, **37,** 2644–2660.

Held, I. M., and E. O'Brien, 1992: Quasigeostrophic turbulence in a three-layer model: Effects of vertical structure in the mean shear. *J. Atmos. Sci.*, **49,** 1861–1870.

Holloway, G., and S. Kristmannsson, 1984: Stirring and transport of tracer fields by geostrophic turbulence. *J. Fluid Mech.*, **141,** 27–50.

Hoyer, J.-M., and R. Sadourny, 1982: Closure modeling of fully developed baroclinic instability. *J. Atmos. Sci.*, **39,** 707–721.

Kraichnan, R. H., 1967: Inertial ranges in two-dimensional turbulence. *Phys. Fluids,* **10,** 1417–1423.

——, 1971: Inertial-range transfer in two- and three-dimensional turbulence. *J. Fluid Mech.*, **47,** 525–535.

Leith, C. E., 1968: Diffusion approximation for two-dimensional turbulence. *Phys. Fluids,* **11,** 671–673.

Lesieur, M., and J. Herring, 1985: Diffusion of a passive scalar in two-dimensional turbulence. *J. Fluid Mech.*, **161,** 77–95.

Maltrud, M. E., and G. K. Vallis, 1991: Energy spectra and coherent structures in forced two-dimensional and beta-plane turbulence. *J. Fluid Mech.*, **228,** 321–342.

Panetta, R. L., 1993: Zonal jets in wide baroclinically unstable regions: Persistence and scale selection. *J. Atmos. Sci.*, **50,** 2073–2106.

Rhines, P. B., 1977: The dynamics of unsteady currents. *The Sea,* Vol. 6, E. A. Goldberg, I. N. McCane, J. J. O'Brien, and J. H. Steele, Eds., Wiley, 189–318.

Salmon, R., 1978: Two-layer quasi-geostrophic turbulence in a simple special case. *Geophys. Astrophys. Fluid Dyn.*, **10,** 25–52.

——, 1980: Baroclinic instability and geostrophic turbulence. *Geophys. Astrophys. Fluid Dyn.*, **15,** 167–211.

Stone, P. H., 1972: A simplified radiative-dynamical model for the static stability of rotating atmospheres. *J. Atmos. Sci.*, **29,** 11–37.

Vallis, G. K., 1983: On the predictability on quasi-geostrophic flow: The effects of beta and baroclinicity. *J. Atmos. Sci.*, **40,** 10–27.